Ferromagneticlike states and all-optical magnetization switching in ferrimagnets

V. N. Gridnev*
Ioffe Physical Technical Institute, RAS, 194021 St. Petersburg, Russia

(Received 14 December 2017; revised manuscript received 11 May 2018; published 24 July 2018)

We study theoretically the light-induced magnetization switching in a binary ferrimagnet of the type A_pB_{1-p}, randomly occupied by two different species of magnetic ions. The localized spins are coupled with spins of itinerant electrons via the *s-d* exchange interaction. The dynamics of the localized and itinerant spins is described by coupled rate equations, which include electron-phonon interaction, spin-lattice relaxation, and exchange scattering, induced by the *s-d* exchange interaction. The exchange scattering leads to the formation of ferromagneticlike states at initial temperatures T both below and above the magnetization compensation temperature T_M with the opposite polarities in these two temperature regions. Inclusion of electron-phonon interaction and spin-lattice relaxation in the dynamical equations leads to the switching in a temperature range $0 < T < T_f$, where T_f is slightly higher than T_M and strongly depends on the spin-lattice relaxation time of itinerant electrons. The switching requires less pulse fluence in the vicinity of T_M.

DOI: 10.1103/PhysRevB.98.014427

I. INTRODUCTION

Since the discovery [1] of all-optical helicity-dependent magnetization switching (AOS) in the ferrimagnetic rare-earth-transition-metal (RE-TM) amorphous GdFeCo alloy film, this phenomenon has attracted a lot of attention. In subsequent experiments AOS was observed not only with circularly polarized light [2,3] but also with linearly polarized light [4–7].

In this paper we will consider heat-induced AOS, whose dependence on helicity is due to magnetic circular dichroism [6]. A distinctive feature of heat-induced AOS is a fast angular momentum transfer between sublattices of the ferrimagnet [8].

AOS was studied theoretically in Refs. [4,5,9–13] using an approach based on the atomistic spin simulations. Atomistic spin models are essentially models of localized spins, coupled by exchange interactions. The temporal evolution of individual atomic spins is governed by the coupled stochastic Landau-Lifshitz-Gilbert (LLG) equations. Although these models demonstrate the possibility of heat-induced switching in ferrimagnets, they do not give any information about the microscopic mechanisms of AOS. These theories do not consider electron-spin coupling explicitly and thus are unable to describe properly the energy and angular momentum transfer between itinerant electrons and localized spins. Being phenomenological, LLG equations are applicable only on a long timescale, when deviation from equilibrium is not too large. In the opposite case, one should solve equations for spin distribution functions (see, e.g., Ref. [14]). This well-known fact has been stressed again in connection with the ultrafast magnetization dynamics [15,16]. In order to understand the microscopic mechanisms of AOS it is necessary to go beyond the framework of the approaches, which operate with localized spins and neglect itinerant ones.

For this reason, in our previous work [17] we studied AOS theoretically, using the *s-d* model, which considers electron-spin coupling explicitly and thus allows one to describe properly the energy and angular momentum transfer between the sublattices. The fundamental mechanism underlying ferromagnetic ordering in the *s-d* model is the exchange coupling between localized and delocalized spins [18–21]. The *s-d* model was applied to the analysis of the laser-induced magnetization dynamics in ferro- and ferrimagnets [22–24].

In Ref. [17] the description of the electron-phonon (*e*-ph) interaction was oversimplified because the peak electron temperature $T_e^{\max}$ was taken as an input parameter. In this paper we essentially modify our previous theoretical consideration of AOS. We include in dynamical equations not only the *e*-ph interaction but also electron cooling due to the *s-d* interaction. Thus, the electron temperature becomes coupled with the spin dynamics. As a result, we clarify the relative role played in AOS by the *s-d* scattering, electron cooling, and spin-lattice relaxation.

This paper is organized as follows. In Sec. II we introduce the *s-d* model for the two-sublattice ferrimagnet and provide equations governing the dynamics. In Sec. III we present solutions of kinetic equations for the spin polarizations of the magnetic sublattices. We discuss how the switching depends on the initial temperature. Section IV concludes the paper.

II. ULTRAFAST MAGNETIZATION DYNAMICS IN THE *s-d* MODEL

A. *s-d* model of a two-sublattice ferrimagnet

In our study we model the RE-TM ferrimagnet by two sublattices of localized spins interacting with itinerant electrons via the *s-d* exchange interaction. Referring to Refs. [17,22] for details, we provide here only key definitions and pay special attention to the modification of our previous study [17].

The degenerate electron gas of density n_c forms a single band with energy $E_{\mathbf{k}s}$, where $\mathbf{k}$ and s are the wave vector and

*gridnev@mail.ioffe.ru

spin, respectively. The exchange interaction between itinerant spins $\mathbf{s}_j$ and localized spins $\mathbf{S}_i$ is given by

$$\hat{H}_{sd} = \sum_{i,j} \alpha_i \delta(\mathbf{r}_j - \mathbf{R}_i)(\hat{\mathbf{S}}_i \cdot \hat{\mathbf{s}}_j), \tag{1}$$

where $\mathbf{r}_j$ ($\mathbf{R}_i$) is the position of the carrier (localized spin) and α_i is the exchange coupling constant of the s-d interaction for spin $\mathbf{S}_i$. A localized spin $\mathbf{S}_i$ possesses $(2S_i + 1)$ discrete energy levels. This model is commonly referred to as the s-d (s-f) model. In the following we assume that all average localized spins are parallel or antiparallel to the z axis.

The s-d interaction can be decomposed into mean-field and fluctuational parts:

$$\hat{H}_{sd} = \hat{H}_{sd}^{mf} + \hat{H}_{sd}^{'}, \tag{2}$$

where

$$\hat{H}_{sd}^{mf} = \sum_i \alpha_i n_c \left[\langle \hat{s}^z(\mathbf{R}_i)\rangle \hat{S}_i^z + \langle \hat{S}_i^z \rangle \hat{s}^z(\mathbf{R}_i)\right], \tag{3}$$

$$\hat{H}_{sd}^{'} = \frac{1}{2}\sum_i \alpha_i n_c [\hat{S}_i^+ \hat{s}^-(\mathbf{R}_i) + \hat{S}_i^- \hat{s}^+(\mathbf{R}_i)], \tag{4}$$

where n_c is the density of itinerant electrons and $\hat{\mathbf{s}}(\mathbf{R}_i) = n_c^{-1}\sum_j \hat{\mathbf{s}}_j \delta(\mathbf{r}_j - \mathbf{R}_i)$ is a reduced spin density. $\hat{H}_{sd}^{mf}$ is diagonal in the $\hat{S}^z$ basis, while $\hat{H}_{sd}^{'}$ is off diagonal. As in ferromagnets [22], the quantity

$$\delta_i = n_c \alpha_i \langle \hat{s}^z(\mathbf{R}_i)\rangle \tag{5}$$

is the energy-level splitting of the localized spin at $\mathbf{R}_i$.

We will study AOS in a binary ferrimagnet of the type A_pB_{1-p}, randomly occupied by two different species of magnetic ions with spins $S_A = 3$ and $S_B = 1$ (in units of $\hbar$), respectively.

We assume homogeneous distribution of average spins over sites of each magnetic sublattice, i.e., $S_{j_\nu}^z = S_\nu^z$ and $s_z(R_{j_\nu}) = s_z(R_\nu)$ for all j_ν, where $\nu = A$ or B and R_ν denotes an arbitrary site in the sublattice ν.

Below T_c the equilibrium values of the localized and itinerant spins obey the relations

$$s_z(R_A) = p\chi_{AA} S_A^z + (1-p)\chi_{AB} S_B^z, \tag{6}$$

$$s_z(R_B) = p\chi_{BA} S_A^z + (1-p)\chi_{BB} S_B^z, \tag{7}$$

where S_ν^z and $s_z(R_\nu)$ are the average localized spin and reduced carrier spin density at R_ν, respectively, and $\chi_{\nu\mu}$ is an electron spin susceptibility. For the following discussion we introduce spin polarizations of the sublattices, $P_A = pS_A^z$, $P_B = (1-p)S_B^z$, and their sum $P = P_A + P_B$.

We consider the susceptibilities χ_{AA}, χ_{BB}, χ_{AB}, and χ_{BA} as input parameters and choose their values to reproduce qualitatively the equilibrium magnetic characteristics of RE-TM alloys.

Note that it is not obvious to consider the spins of transition-metal ions as localized since magnetization arises from a significant portion of itinerant electrons. The application of the s-d model to the RE-TM ferrimagnets is allowed only if we consider itinerant electron states near the Fermi energy ($E_F \pm kT_e$). The s-d model cannot be used for a calculation of the electron spin susceptibilities $\chi_{\mu\nu}$ in Eqs. (6) and (7). For this reason we consider $\chi_{\mu\nu}$ as input parameters. The choice of the s-d model allows us to study the ultrafast dynamics at finite temperatures (due to the presence of local moments) and to take into account the band electrons.

Since our goal here is to establish a connection between the results of the model calculation and experimental observation of AOS, we point out the relationship between our model and the electronic structure of GdFeCo. The $4f$ electrons of rare-earth ions are localized and form the localized spin system A. System B is formed by semilocalized $3d$ electrons of Fe and Co. Due to the dual property of the $3d$ electrons [25] they also contribute to the itinerant electron states. In GdFeCo the itinerant electrons are originated from the $3d$ electrons hybridized with Gd $5d$ electrons. The contribution of sp electrons to the itinerant states is relatively small [26]. Thus, in our model the "s electrons" correspond to the hybridized $3d$ and $5d$ electrons in GdFeCo. Due to the hybridization it is possible to consider these two subsystems as one shared system. The $3d$-$5d$ hybridization is responsible for the coupling between the Gd and FeCo moments. The FeCo magnetic moments are ferrimagnetically aligned to the Gd ones via $4f$-$5d$ ferromagnetic exchange coupling and $3d$-$5d$ hybridization [27,28].

B. Dynamic equations

After the photoexcitation, the nonequilibrium electrons can be described by a Fermi-Dirac function with an electron temperature $T_e(t)$ and spin-dependent chemical potentials $\mu_s(t)$:

$$f_s(E) = \frac{1}{1 + e^{(E-\mu_s)/k_B T_e}}. \tag{8}$$

The average localized spins are determined by the equation $S_\nu^z = \sum_m m\rho_m^\nu$, where ρ_m^ν are the populations (diagonal elements of the density matrix $\hat{\rho}^\nu$) of the Zeeman spin states, $-S_\nu \leqslant m \leqslant S_\nu$.

The electron temperature T_e is related to the dynamics of spin and phonon systems by the equations

$$C_e(T_e)\frac{dT_e}{dt} = -G_{ep}(T_e - T_p) - \Gamma_{es} + P(t), \tag{9}$$

$$C_p\frac{dT_p}{dt} = G_{ep}(T_e - T_p) - \frac{T_p - T}{\tau_p}, \tag{10}$$

where T is the initial temperature, $T_p(t)$ is the phonon temperature, G_{ep} is the electron-phonon coupling, $P(t) = P_0\exp[-(t/t_0)^2]$ describes the time evolution of the laser energy transfer to the electrons, and Γ_{es} is the rate of energy transfer between electrons and localized spins. Typically, this value is calculated by the second-order perturbation theory [29,30]. Since we neglect the direct interaction of localized spins with phonons, the rate Γ_{es} can be calculated as

$$\Gamma_{es} = \frac{dE_s}{dt}, \tag{11}$$

where $E_s = n_A\delta_A P_A + n_B\delta_B P_B$ is the energy density of the spin system. Here n_A and n_B are the densities of the localized spins. The last term in Eq. (10) describes heat diffusion to an environment.

Note that we do not consider the peak electron temperature $T_e^{\max}$ as an input parameter. Since our purpose here is to study the temperature dependence of the switching, we will take the laser pulse fluence $F_0 = P_0 t_0 \sqrt{\pi}$ as an input parameter and then calculate $T_e(t)$ and $T_e^{\max}$. Both these quantities are coupled with the spin dynamics (see below).

The populations ρ_m^ν obey the rate equations [22,31,32]

$$\frac{d\,\rho_m^\nu}{dt} = -\left(w_{m-1,m}^\nu + w_{m+1,m}^\nu\right)\rho_m^\nu + w_{m,m+1}^\nu \rho_{m+1}^\nu + w_{m,m-1}^\nu \rho_{m-1}^\nu, \tag{12}$$

where $w_{n,m}^\nu$ is the transition rate from the mth to nth energy level of the localized spins belonging to the ν sublattice:

$$w_{m,m\pm1}^\nu = C_\nu S_{m,m\pm1}^{\nu\mp} \frac{\beta_e(\pm\delta_\nu + \mu_s - \mu_{s'})}{1 - \exp[\beta_e(\mp\delta_\nu - \mu_s + \mu_{s'})]}, \tag{13}$$

where $S_{m,m\pm1}^{\nu\mp} = S_\nu(S_\nu+1) - m(m\pm1)$, $s = \mp\frac{1}{2}$, $s' = \pm\frac{1}{2}$, $\beta_e = 1/k_B T_e(t)$. The coefficients C_ν are determined by the electronic structure and parameters of the s-d interaction α_A and α_B in Eq. (1) (see the Appendix of Ref. [17] for details). Note that the parameters β_e, δ_ν, and μ_s in Eq. (13) vary with time.

In Eq. (13) we neglect the direct spin-lattice relaxation of localized spins. Ignoring this relaxation mechanism is not a rough approximation. Since the paper by Mitchel [33], the dominant view is that in transition metals the loss of energy and angular momentum from localized spins is mostly determined by the s-d interaction combined with the relaxation of itinerant spins to the lattice. Such simplification is justified for GdFeCo since the Gd orbital angular momentum is zero, but it is questionable for the TbFeCo and DyFeCo alloys because spin-lattice coupling of Tb and Dy is stronger than that of Gd.

The spin splitting of the carriers' chemical potential $\Delta\mu = \mu_\uparrow - \mu_\downarrow$ is given by

$$\mu_\uparrow - \mu_\downarrow = n_c(s_z - s_{ie})\frac{D_\uparrow(E_F) + D_\downarrow(E_F)}{D_\uparrow(E_F) D_\downarrow(E_F)}, \tag{14}$$

where $D_s(E_F)$ is the spin-resolved density of states at the Fermi level and $s_{ie}(t)$ is an instantaneous equilibrium value of the average electron spin s_z, determined by the electron temperature T_e and by the condition $\mu_\uparrow = \mu_\downarrow$. We define s_{ie} from physical considerations:

$$s_{ie}(t) = p\, s_z(R_A, t) + (1-p) s_z(R_B, t), \tag{15}$$

where $s_z(R_A)$ and $s_z(R_B)$ are given by Eqs. (6) and (7) with time-dependent S_A^z and S_B^z.

The dynamics of the average itinerant spin, entering Eq. (14), is determined by the exchange scattering and spin-lattice relaxation

$$\frac{ds_z}{dt} = -\frac{n_A}{n_c}\frac{dS_A^z}{dt} - \frac{n_B}{n_c}\frac{dS_B^z}{dt} - \frac{[s_z - s_{ie}(t)]}{\tau_{sl}}. \tag{16}$$

The first two terms on the right-hand side describe the exchange scattering, and the third term describes the spin-lattice relaxation of the average electron spin with a relaxation time τ_{sl}. Spin-lattice relaxation times τ_{sl} in magnetic and nonmagnetic metals do not differ significantly because they are mainly determined by the spin-orbit interaction.

Thus, the nonequilibrium state is characterized by the electron and phonon temperatures $T_e(t)$ and $T_p(t)$, respectively, and by the average localized and itinerant spins, $S_\nu^z(t)$ and $s_z(t)$. The dynamics of these variables is governed by Eqs. (9), (10), (12), and (16) together with Eqs. (11), (13), (14), and (15). Note that our theory operates with spins rather than magnetic moments since the exchange interaction plays a more important role in the switching than the interaction with an external magnetic field.

In the following numerical calculations we always assume a common initial temperature of electrons and phonons, $T_e = T_p = T$, before laser excitation. Initial values of spin populations are equal to their equilibrium values, which are calculated by the standard mean-field theory, as was done in Ref. [17].

Note that, typically, the cooling of electrons due to the energy flux Γ_{es}, Eq. (11), is neglected. This is justified when the peak electron temperature $T_e^{\max}$ is considered an input parameter. In our calculations we take the laser pulse fluence $F_0 = P_0 t_0 \sqrt{\pi}$ as an input parameter and then calculate $T_e(t)$ and $T_e^{\max}$. The strong magnitude of the exchange interaction (1) leads to a significant reduction of $T_e^{\max}$, i.e., energy transfer from hot electrons to localized spins influences $T_e^{\max}$. For this reason we include the energy flux Γ_{es} in Eq. (9).

All parameters used in the numerical calculation can be divided into three groups:

(1) Parameters of the s-d model were chosen to qualitatively describe equilibrium magnetic properties of the GdFeCo system. For numerical estimates we use the following parameter values: $p = 0.35$, $\chi_{AA} = \chi_{BB} = 1$, $\chi_{AB} = -1$, $\chi_{BA} = -0.1$, $n_c = 10^{23}$ cm^{-3}, $n_c\alpha_A = 0.01$ eV, and $n_c\alpha_B = 0.1$ eV. Concentrations of A and B spins are $n_A = p n_c$ and $n_A = (1-p)n_c$. For these parameters the Curie temperature $T_C = 526$ K, and the magnetic compensation temperature $T_M = 267$ K. Thus, the equilibrium magnetic properties of our model are qualitatively similar to those of the GdFeCo ferrimagnetic alloys [34].

(2) Additional parameters are needed for the calculation of the temporal behavior of P_A, P_B, and s_z. We choose the specific heat of the phonons $C_p = 3 \times 10^6$ J m^{-3} K^{-1} and the electrons $C_e = \gamma T_e$, where $\gamma = 700$ J m^{-3} K^{-2}, the e-ph coupling $G_{ep} = 1 \times 10^{17}$ W m^{-3} K^{-1}. These numerical values were chosen in Ref. [35] to obtain a quantitative agreement between calculations and the experiment on demagnetization (not switching) in the GdFeCo system. Assuming equal densities of states for both spins, $D_\uparrow(E_F) = D_\downarrow(E_F) \equiv D$, and using the relation $\gamma = \frac{1}{3}\pi^2 k_B^2 D$, we obtain $D = 1.76 \times 10^{23}$ cm^{-3} eV^{-1}.

We have not found any data in the literature on the magnitude of the spin-lattice relaxation time of itinerant electrons in GdFeCo. This time is difficult to measure in ferromagnets, especially if it is in the subpicosecond range. To separate contributions of itinerant and localized spins to the relaxation one needs to exploit spin-dependent transport. We are aware of only a few articles reporting such measurements [36–38]. These experiments give rather small τ_{sl} of the order of 0.1 ps. From a theoretical point of view there are two factors which significantly accelerate the spin-lattice relaxation of itinerant electrons in GdFeCo. (i) For a large concentration of heavy

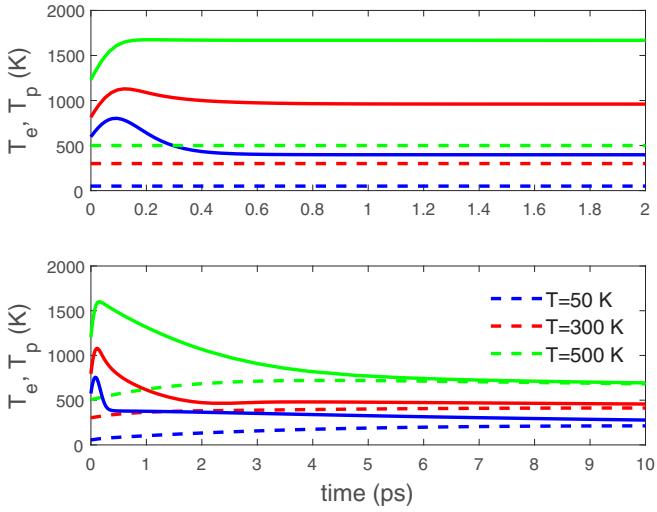

FIG. 1. Calculated time evolution of T_e (solid lines) and T_p (dashed lines) after laser excitation at three different initial temperatures. $G_{ep} = 0$ (top panel) and $G_{ep} = 4 \times 10^{17}$ W m^{-3} K^{-1} (bottom panel).

ions (Gd), a strong electric field caused by nuclei of the heavy ions increases spin-orbit splitting of the itinerant electrons, thus leading to a sizable change in electron spin at every scattering event. (ii) Due to the amorphous structure of GdFeCo alloys, constraints imposed on the spin-independent scattering by quasimomentum conservation are removed [37]. The combined impact of factors (i) and (ii) strongly accelerates the spin-lattice relaxation. Relying on the physical consideration and the experimental studies [36–38], we set the spin-lattice relaxation time $\tau_{sl} = 0.1$ ps.

The coefficients C_A and C_B in Eq. (13) determine the exchange scattering rates of A and B spins, respectively. We set the numerical values of these parameters from physical considerations. From the relations $C_A \propto \alpha_A^2$, $C_B \propto \alpha_B^2$, and $\alpha_B \gg \alpha_A$ it follows that $C_A \ll C_B$. Therefore, the rate of angular momentum transfer between the sublattices is mainly determined by C_A. We assume that the switching time $t_{sw} \sim C_A^{-1}$ if numerical values of other parameters are most favorable for the switching. On this basis, we set $C_A = 1$ ps^{-1}, $C_B = 10$ ps^{-1}.

(3) Other parameters are determined by experimental conditions and sample design. These are the pulse duration and fluence and the heat diffusion time. We set the pulse duration $t_0 = 100$ fs and the heat diffusion time $\tau_p = 20$ ps. The calculations are performed for different values of laser fluence F_0.

Figure 1 shows the calculated temporal behavior of the electron and phonon temperatures for different initial temperatures and e-ph coupling. The top panel demonstrates the electron cooling without the e-ph interaction due to the energy flux Γ_{es}.

III. RESULTS

In this section we present numerical solutions of the dynamic equations and clarify the role of the exchange scattering, e-ph interaction, and spin-lattice relaxation in AOS. To this end, we first consider the dynamics without the e-ph interaction and spin-lattice relaxation ($G_{ep} = 0, \tau_{sl} = \infty$), i.e., the dynamics governed only by the exchange scattering (Sec. III A). Note that electron cooling still occurs (Fig. 1). Then we include in the consideration the e-ph interaction (Sec. III B), and finally, we add the spin-lattice relaxation in Sec. III C.

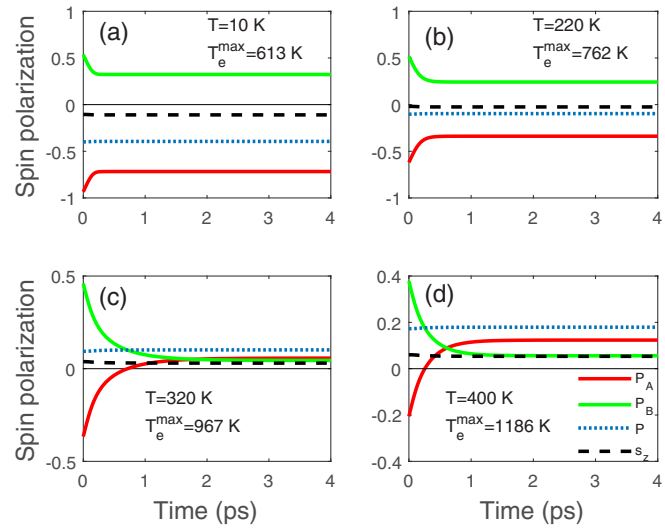

FIG. 2. Computed dynamics of localized and itinerant spins in $A_{35}B_{65}$ without e-ph interaction for different initial temperatures (a) and (b) below and (c) and (d) above compensation temperature $T_M \approx 267$ K. The pulse fluence $F_0 = 0.8$ GJ m^{-3}.

A. Ferromagneticlike state and exchange scattering

Figures 2 and 3 show temporal behavior of spin polarizations at different initial temperatures and pulse fluences $F_0 = 0.8$ and 1.2 GJ m^{-3}, respectively. At a fixed pulse fluence the peak electron temperature $T_e^{\max}$ increases with the initial temperature T. The rise of electron temperature ($T_e^{\max} - T$)

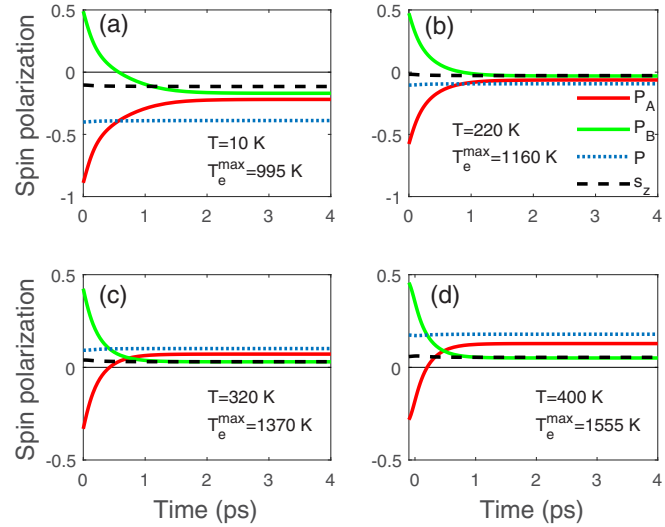

FIG. 3. Computed dynamics of localized and itinerant spins in $A_{35}B_{65}$ without e-ph interaction for different initial temperatures (a) and (b) below and (c) and (d) above compensation temperature $T_M \approx 267$ K. The pulse fluence $F_0 = 1.2$ GJ m^{-3}.

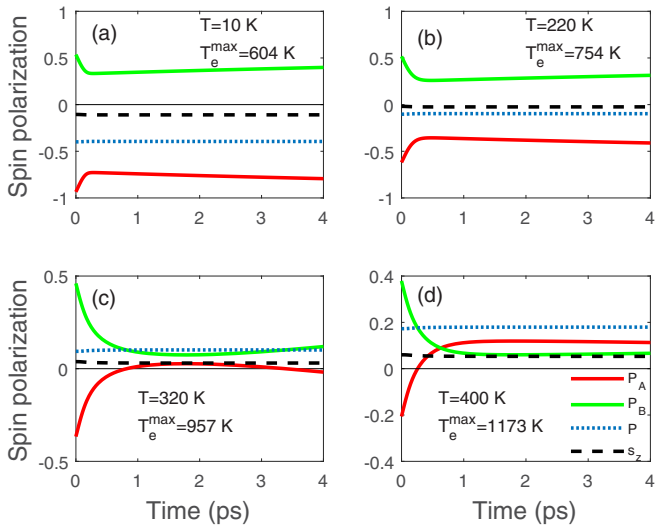

FIG. 4. Demagnetization and recovery for different initial temperatures (a) and (b) below and (c) and (d) above the compensation temperature. The electron-phonon coupling $G_{ep} = 1 \times 10^{17}$ W m^{-3} K^{-1} and pulse fluence $F_0 = 0.8$ GJ m^{-3}.

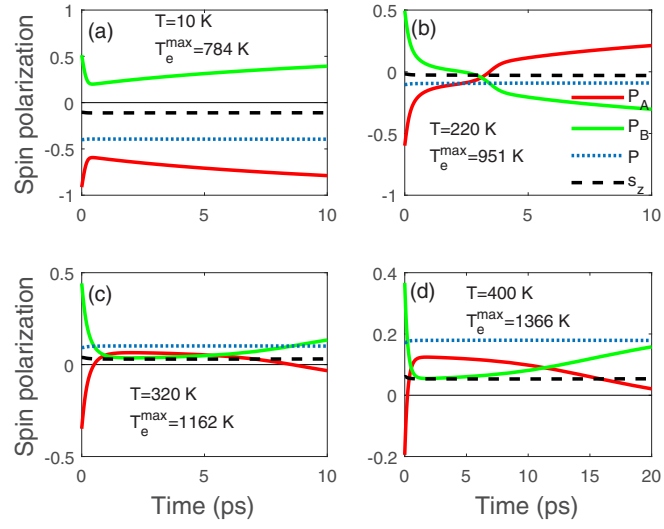

FIG. 5. (b) Ultrafast switching and (a), (c), and (d) recovery for different initial temperatures (a) and (b) below and (c) and (d) above the compensation temperature. The electron-phonon coupling $G_{ep} = 1 \times 10^{17}$ W m^{-3} K^{-1} and pulse fluence $F_0 = 1.0$ GJ m^{-3}.

slowly increases with T since cooling of electrons due to the exchange scattering is less effective at high temperatures.

In equilibrium ($t < 0$), $|P_A| > |P_B|$ below T_M, and $|P_A| < |P_B|$ above T_M (similar relations hold between magnetizations of Gd and Fe sublattices in Gd-Fe alloys).

After heating of electrons by a laser pulse, P_A and P_B vary with time due to the exchange scattering and in the absence of the e-ph interaction and spin-lattice relaxation approach to new quasiequilibrium values. As seen from Figs. 2 and 3, the electron spin polarization s_z changes little over time. Thus, we conclude that P_A and P_B vary with time due to angular momentum exchange between the sublattices. For this reason

$$\frac{dP_A}{dt} \simeq -\frac{dP_B}{dt}. \tag{17}$$

This equation means that the sublattice spin polarizations $P_\nu(t)$ vary with nearly equal rates. This does not contradict the experiment [4]. Since $|P_B| < |P_A|$ at $T < T_M$, P_B reaches zero before P_A, eventually leading to the onset of the ferromagneticlike state (FLS) where the two sublattices align parallel. The polarities of the FLS at $T > T_M$ and $T < T_M$ are opposite since the polarity is determined by the sign of the difference $|P_B| - |P_A|$.

For a given initial temperature T, the FLS appears when the fluence exceeds a certain value $F_0(T)$. When the fluence increases, the FLS first appears at initial temperatures just below the Curie temperature. For larger fluences the FLS also appears at lower initial temperatures. A further increase in the fluence leads to the demagnetization without any qualitative changes in temporal dynamics.

Note that the formation of the FLS in the absence of dissipation can also be obtained in a localized spin model [9]. In the modeling of Ref. [39] there is a change in polarity of the FLS but for initial temperatures close to T_C, not above T_M. Most likely, this discrepancy with our results is caused by different modeling of laser heating. Here we calculate the dependence on the initial temperature for fixed laser fluences, while in Ref. [39] such calculations were performed for fixed maximum electron temperatures $T_e^{\max}$.

Here we pay special attention to the formation of FLS in order to show in the following how the e-ph interaction affects this process.

B. Electron-phonon interaction and exchange scattering

The e-ph interaction significantly affects the dynamics described in the previous section. Depending on the e-ph coupling, initial temperature, and pulse fluence, one can observe the magnetization switching or recovery.

Figure 4 demonstrates the influence of the e-ph interaction on the spin dynamics at low fluence. As expected, all stationary quasiequilibrium states shown in Fig. 2 recover to the initial state. The stationary FLSs [Figs. 2(c) and 2(d)] transform to the transient ones [Figs. 4(c) and 4(d)].

The switching arises at initial temperatures just below T_M when the fluence exceeds a certain critical value, but above T_M the transient FLS recovers to the initial state (Fig. 5). A further increase in the fluence leads to the switching at lower temperatures (Fig. 6), but above T_M the switching does not occur. Thus, the formation of transient FLS is not sufficient for the switching.

It is interesting to see how such dynamical behavior transforms with a variation of the e-ph coupling. It is obvious that too strong e-ph coupling is not favorable for the formation of FLS. We perform calculations for the fixed pulse fluence $F_0 = 1.2$ GJ m^{-3} (as in Fig. 6) and varying G_{ep} and find that FLS occurs when $G_{ep} \lesssim 3 \times 10^{17}$ W m^{-3} K^{-1} (not shown). As F_0 increases, formation of FLS becomes allowed with stronger e-ph coupling. A comparison of Figs. 6 and 7 shows that a moderate increase in the pulse fluence leads to the formation of FLS at considerably higher values of G_{ep}.

Thus, our theory predicts that without the spin-lattice relaxation the switching occurs only at initial temperatures below T_M. The switching requires smaller pulse fluence at initial

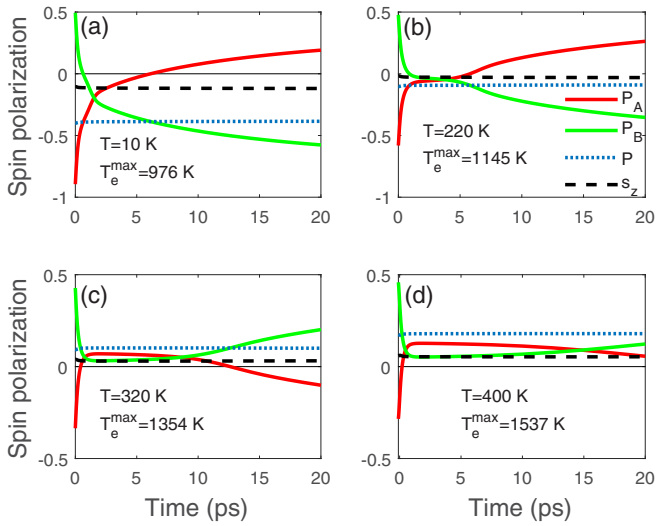

FIG. 6. (a) and (b) Ultrafast switching and (c) and (d) recovery for different initial temperatures (a) and (b) below and (c) and (d) above the compensation temperature. The electron-phonon coupling $G_{ep} = 1 \times 10^{17}$ W m^{-3} K^{-1} and pulse fluence $F_0 = 1.2$ GJ m^{-3}.

temperatures in the vicinity of T_M. At initial temperatures above T_M the switching does not occur.

A possible reason for the significant difference in the temporal behavior of P_ν below and above T_M is that the transfer of angular momentum and energy between the sublattices are coupled. In order to meet the requirements imposed by the laws of conservation of energy and angular momentum, there should be a certain relationship between spin splittings and spin polarizations of the sublattices. The spin splitting of B spins (TM) significantly exceeds the splitting of A spins (RE), i.e., $|\delta_B| > |\delta_A|$ at all initial temperatures below T_C. This relation between δ_B and δ_A does not change as T goes through T_M. In contrast, the relation between P_B and P_A changes at

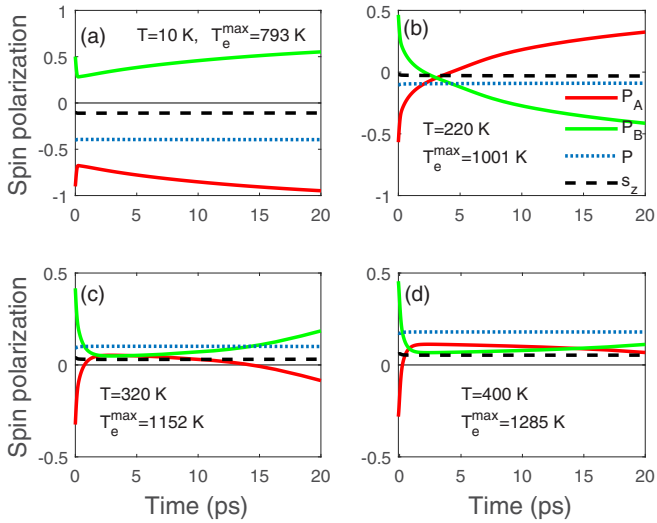

FIG. 7. (b) Ultrafast switching and (a), (c), and (d) recovery for different initial temperatures (a) and (b) below and (c) and (d) above the compensation temperature. The electron-phonon coupling $G_{ep} = 100 \times 10^{17}$ W m^{-3} K^{-1} and pulse fluence $F_0 = 2$ GJ m^{-3}.

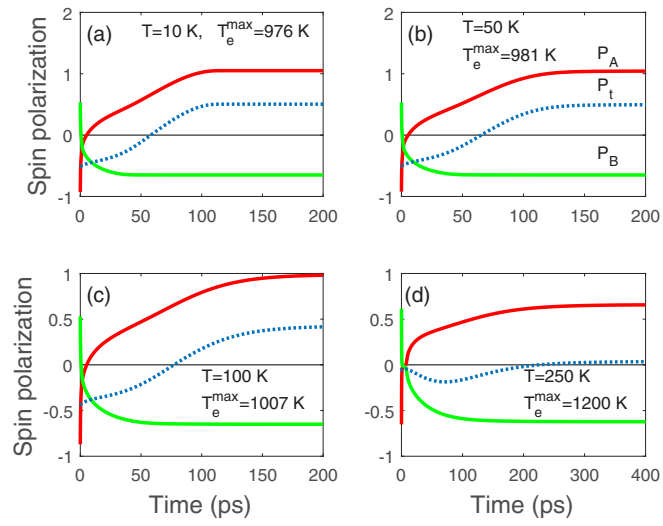

FIG. 8. Ultrafast switching of the spin polarizations P_A, P_B, and $P_t = P_A + P_B + s_z$ for different initial temperatures below the compensation temperature, with the electron spin-lattice relaxation time $\tau_{sl} = 0.1$ ps. The parameters G_{ep} and F_0 are the same as in Fig. 6.

T_M: $|P_B| < |P_A|$ for $T < T_M$, but $|P_B| > |P_A|$ for $T > T_M$. Since the transfer of angular momentum and energy between the sublattices are coupled, the exchange scattering is more effective when $|P_B| < |P_A|$ and $|\delta_B| > |\delta_A|$, that is, at $T < T_M$.

Note that since we neglect the spin-lattice relaxation, the switching which we observe below T_M is still incomplete [17]. This is because the total angular momentum of the localized and itinerant spins $P_A + P_B + s_z$ is conserved. Both P_A and P_B change their signs with time and approach quasiequilibrium values. In this process $P_A + P_B \approx$ const since $s_z \ll P_A + P_B$. Such a process is not switching in the strict sense. We will call it incomplete switching. Thus, the conservation of angular momentum in the absence of the spin-lattice relaxation prevents complete switching. Below we consider the influence of the spin-lattice relaxation on the dynamics.

C. Spin-lattice relaxation

Based on the above consideration, we expect that below T_M the spin-lattice relaxation will lead to the transformation of the incomplete switching to the complete one. Numerical calculations confirm this assumption (see Fig. 8). As seen in Fig. 8, immediately after the photoexcitation, the exchange scattering causes the relatively fast angular momentum transfer between the sublattices until the complete switching of the B sublattice. This asymmetry in behavior of A and B sublattices is due to the inequality $|P_B| < |P_A|$ below T_M. The duration of this stage is approximately the same both with and without the spin-lattice relaxation (Fig. 6 shows the dynamics on a shorter timescale). Without the spin-lattice relaxation the first stage is also the final stage. If the relaxation of itinerant spins occurs, the A sublattice continues the switching until it switches completely on a longer timescale. The duration of this timescale depends on τ_{sl}. Thus, below T_M the complete reversal of A and B sublattices occurs on distinctly different timescales. This means that below T_M, the A (RE) sublattice is "slower"

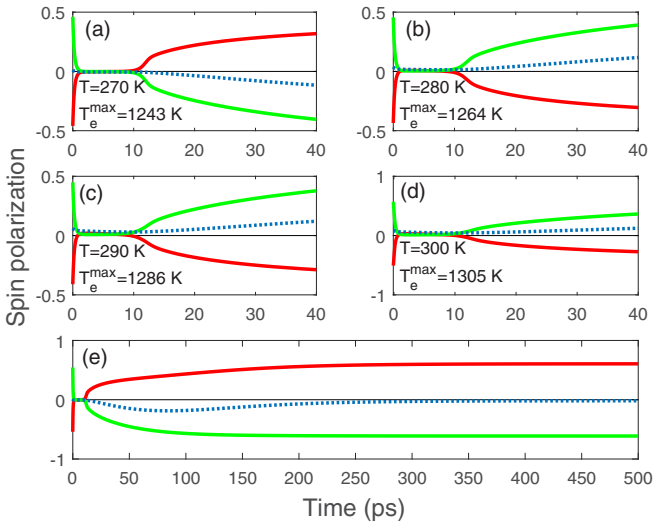

FIG. 9. (a) and (e) Ultrafast switching and (b)–(d) recovery of the spin polarizations P_A (red solid line), P_B (green solid line), and $P_t = P_A + P_B + s_z$ (blue dotted line) for different initial temperatures above the compensation temperature, with the electron spin-lattice relaxation time $\tau_{sl} = 0.1$ ps. (e) shows the same dynamics as (a) but at longer times. The parameters G_{ep} and F_0 are the same as in Fig. 6.

than the B (TM) sublattice on both short and long timescales. When the initial temperature approaches the compensation point, P_B approaches P_A, and the switching times of both sublattices become comparable.

The spin-lattice relaxation qualitatively changes the dynamics above T_M. As seen from Fig. 9, the switching appears above T_M but only close to it; that is, the switching occurs in a temperature interval $T_M < T < T_f$, where T_f is a complicated function of τ_{sl} and other parameters of the model. Varying these parameters, we were unable to get $T_f > 340$ K. Again, one can see fast dynamics due to the exchange scattering and subsequent slow variation due to other interactions.

Figure 8 demonstrates that the net spin polarization crosses zero on a significantly longer timescale than the corresponding timescales for sublattice magnetizations (Fig. 6). It is seen from Fig. 6 that the switching times of sublattice magnetizations are in the range from 1 to 5 ps. Therefore, the switching time measured experimentally can be highly dependent on what is probed in the experiment. In general, both sublattices contribute to the Kerr rotation in the optical experiments, but the relative contributions of the sublattices depend on the wavelength of light [40] and, probably, on the chemical composition of the RE-TM alloys.

IV. CONCLUSIONS

During the past decade AOS has been the subject of many experimental and theoretical studies. Now, it has become clear that the lack of clarity in the understanding of the microscopic mechanisms of AOS is due to the complicated interplay of different interactions and relaxation processes responsible for the switching. To separate the contributions of different processes to AOS and understand better their role in the switching, we studied AOS in the two-sublattice ferrimagnet described by the *s-d* model. The model comprises three spin species: two sublattices of localized spins, interacting with itinerant spins via the *s-d* exchange interaction. This model allows one to describe the angular momentum transfer between the sublattices more exactly than localized spin models.

The spin dynamics is governed by three different processes: the *s-d* exchange scattering, electron-phonon interaction, and spin-lattice relaxation. Depending on the parameters of the model, our theory describes the demagnetization, transient FLS, and/or switching. The exchange scattering alone, i.e., the electron-spin scattering without the electron-phonon interaction and spin-lattice relaxation, leads to the formation of FLS at any initial temperature $T < T_C$ both below and above T_M. The lower the initial temperature is, the greater the fluence needed to create FLS is. FLSs below and above T_M have opposite polarities.

The inclusion of the *e*-ph interaction in the dynamics equations leads to the switching just below T_M when the fluence exceeds a certain critical value. For larger fluences the switching also occurs at lower temperatures. Above T_M the switching does not occur.

Without the spin-lattice relaxation the net angular momentum is conserved. Therefore, the sublattice spin polarizations change over time with the same rates, and the switching is incomplete.

The spin-lattice relaxation leads to the appearance of the switching above T_M in the temperature interval $T_M < T < T_f$, where T_f is slightly higher than the compensation temperature and depends on the parameters of the model. Above T_f the transient FLS occurs, but the switching does not.

Our theory predicts that the switching requires less pulse fluence in the vicinity of T_M. The studies of AOS utilizing localized spin models [13,41] came to a similar conclusion: the presence of T_M is not absolutely necessary, but the most efficient switching happens in the vicinity of T_M. Experimental data on AOS, summarized in Ref. [42], indicate that a low-remanent sample magnetization M_R is crucial for AOS in ferrimagnets.

A distinctive feature of the dependence of the switching on the initial temperature obtained in this paper is its asymmetry with respect to the compensation temperature T_M. While the switching is possible at any initial temperature below T_M, above T_M it occurs in the temperature interval $T_M < T < T_f$. The theoretical study of the switching based on exchange-coupled carrier dynamics [24] predicts the occurrence of the switching only below T_M. Such asymmetry was observed in experimental studies of the switching in GdFeCo [3,43–45], where strong changes in the magnetization dynamics have been observed when the initial temperature crosses T_M. To facilitate a comparison of our results with the experimental data, we provide here quotes from these articles.

Vahaplar *et al.* [3] state, "the optimal conditions for the all-optical reversal are achieved just below the ferrimagnetic compensation temperature. ...Although the all-optical reversal can be observed above and below the compensation temperature of ferrimagnetic GdFeCo alloys, in the vicinity of T_M, the reversal requires less laser pulse fluence. Moreover, the all-optical reversal disappears if the sample temperature is too high above the compensation temperature."

Medapalli *et al.* conclude, "the most efficient demagnetization is achieved when the sample temperature is below

TM and the magnetizations of the sublattices are comparable" [43]. "For a fixed energy of the laser pulse, the dynamics of magnetization showed different behavior depending on whether the sample temperature was below or above the magnetization compensation point (T_M). The conditions for full ultrafast demagnetization and magnetization reversal were easily achieved below T_M, while the same laser excitation caused just 50% demagnetization above T_M" [44].

Le Guyader *et al.* [45] state, "there exists a clear difference between switching below and above T_M. ...The AOS fluence switching window is thus reduced above T_M, and this asymmetry of the switching window around T_M is consistent with the literature."

We stress again that the presented theory is applicable only to Gd-based alloys since the single-pulse, heat-induced switching is experimentally confirmed only in these alloys.

ACKNOWLEDGMENTS

This research was supported by the Russian Science Foundation, Grant No. 16-12-10456.

[1] C. D. Stanciu, F. Hansteen, A. V. Kimel, A. Kirilyuk, A. Tsukamoto, A. Itoh, and T. Rasing, Phys. Rev. Lett. **99**, 047601 (2007).
[2] K. Vahaplar, A. M. Kalashnikova, A. V. Kimel, D. Hinzke, U. Nowak, R. Chantrell, A. Tsukamoto, A. Itoh, A. Kirilyuk, and T. Rasing, Phys. Rev. Lett. **103**, 117201 (2009).
[3] K. Vahaplar, A. M. Kalashnikova, A. V. Kimel, S. Gerlach, D. Hinzke, U. Nowak, R. Chantrell, A. Tsukamoto, A. Itoh, A. Kirilyuk, and T. Rasing, Phys. Rev. B **85**, 104402 (2012).
[4] I. Radu, K. Vahaplar, C. Stamm, T. Kachel, N. Pontius, H. Dürr, T. Ostler, J. Barker, R. Evans, R. Chantrell *et al.*, Nature (London) **472**, 205 (2011).
[5] T. A. Ostler, J. Barker, R. F. L. Evans, R. W. Chantrell, U. Atxitia, O. Chubykalo-Fesenko, S. E. Moussaoui, L. L. Guyader, E. Mengotti, L. J. Heyderman, F. Nolting, A. Tsukamoto, A. Itoh, D. Afanasiev, B. A. Ivanov, A. M. Kalashnikova, K. Vahaplar, J. Mentink, A. Kirilyuk, T. Rasing, and A. V. Kimel, Nat. Commun. **3**, 666 (2012).
[6] A. R. Khorsand, M. Savoini, A. Kirilyuk, A. V. Kimel, A. Tsukamoto, A. Itoh, and T. Rasing, Phys. Rev. Lett. **108**, 127205 (2012).
[7] J. Gorchon, R. B. Wilson, Y. Yang, A. Pattabi, J. Y. Chen, L. He, J. P. Wang, M. Li, and J. Bokor, Phys. Rev. B **94**, 184406 (2016).
[8] J. H. Mentink, J. Hellsvik, D. V. Afanasiev, B. A. Ivanov, A. Kirilyuk, A. V. Kimel, O. Eriksson, M. I. Katsnelson, and T. Rasing, Phys. Rev. Lett. **108**, 057202 (2012).
[9] S. Wienholdt, D. Hinzke, K. Carva, P. M. Oppeneer, and U. Nowak, Phys. Rev. B **88**, 020406 (2013).
[10] R. Chimata, L. Isaeva, K. Kádas, A. Bergman, B. Sanyal, J. H. Mentink, M. I. Katsnelson, T. Rasing, A. Kirilyuk, A. Kimel, O. Eriksson, and M. Pereiro, Phys. Rev. B **92**, 094411 (2015).
[11] O. J. Suarez, P. Nieves, D. Laroze, D. Altbir, and O. Chubykalo-Fesenko, Phys. Rev. B **92**, 144425 (2015).
[12] U. Atxitia, T. A. Ostler, R. W. Chantrell, and O. Chubykalo-Fesenko, Appl. Phys. Lett. **107**, 192402 (2015).
[13] R. Moreno, T. A. Ostler, R. W. Chantrell, and O. Chubykalo-Fesenko, Phys. Rev. B **96**, 014409 (2017).
[14] A. Akhiezer, V. Baryakhtar, and S. Peletminskii, *Spin Waves* (North Holland, Amsterdam, 1968).
[15] P. Nieves, D. Serantes, U. Atxitia, and O. Chubykalo-Fesenko, Phys. Rev. B **90**, 104428 (2014).
[16] P. Nieves, D. Serantes, and O. Chubykalo-Fesenko, Phys. Rev. B **94**, 014409 (2016).
[17] V. Gridnev, J. Phys.: Condens. Matter **28**, 476007 (2016).
[18] C. Zener, Phys. Rev. **81**, 440 (1951).
[19] T. Kasuya, Prog. Theor. Phys. **16**, 45 (1956).
[20] K. Yosida, Phys. Rev. **106**, 893 (1957).
[21] S. V. Vonsovskii, *Magnetism* (Wiley, New York, 1974).
[22] L. Cywiński and L. J. Sham, Phys. Rev. B **76**, 045205 (2007).
[23] V. N. Gridnev, Phys. Rev. B **88**, 014405 (2013).
[24] A. Baral and H. C. Schneider, Phys. Rev. B **91**, 100402 (2015).
[25] T. Moriya, *Spin Fluctuations in Itinerant Electron Magnetism*, Springer Series in Solid-State Sciences (Springer, Berlin, 1985).
[26] H. Tanaka, S. Takayama, and T. Fujiwara, Phys. Rev. B **46**, 7390 (1992).
[27] M. Brooks, Mat. Fys. Medd. K. Dan. Vidensk. Selsk. **45**, 291 (1997).
[28] O. S. Anilturk and A. R. Koymen, Phys. Rev. B **68**, 024430 (2003).
[29] B. König, I. A. Merkulov, D. R. Yakovlev, W. Ossau, S. M. Ryabchenko, M. Kutrowski, T. Wojtowicz, G. Karczewski, and J. Kossut, Phys. Rev. B **61**, 16870 (2000).
[30] A. Manchon, Q. Li, L. Xu, and S. Zhang, Phys. Rev. B **85**, 064408 (2012).
[31] C. P. Slichter, *Principles of Magnetic Resonance* (Springer, Berlin, 1996).
[32] K. Blum, *Density Matrix Theory and Applications* (Springer, Berlin, 2013).
[33] A. H. Mitchell, Phys. Rev. **105**, 1439 (1957).
[34] T. A. Ostler, R. F. L. Evans, R. W. Chantrell, U. Atxitia, O. Chubykalo-Fesenko, I. Radu, R. Abrudan, F. Radu, A. Tsukamoto, A. Itoh, A. Kirilyuk, T. Rasing, and A. Kimel, Phys. Rev. B **84**, 024407 (2011).
[35] A. Mekonnen, A. R. Khorsand, M. Cormier, A. V. Kimel, A. Kirilyuk, A. Hrabec, L. Ranno, A. Tsukamoto, A. Itoh, and T. Rasing, Phys. Rev. B **87**, 180406 (2013).
[36] G.-M. Choi, C.-H. Moon, B.-C. Min, K.-J. Lee, and D. G. Cahill, Nat. Phys. **11**, 576 (2015).
[37] S. Bonetti, M. C. Hoffmann, M.-J. Sher, Z. Chen, S.-H. Yang, M. G. Samant, S. S. P. Parkin, and H. A. Dürr, Phys. Rev. Lett. **117**, 087205 (2016).
[38] G.-M. Choi and B.-C. Min, Phys. Rev. B **97**, 014410 (2018).
[39] U. Atxitia, J. Barker, R. W. Chantrell, and O. Chubykalo-Fesenko, Phys. Rev. B **89**, 224421 (2014).
[40] A. R. Khorsand, M. Savoini, A. Kirilyuk, A. V. Kimel, A. Tsukamoto, A. Itoh, and T. Rasing, Phys. Rev. Lett. **110**, 107205 (2013).
[41] J. Barker, U. Atxitia, T. A. Ostler, O. Hovorka, O. Chubykalo-Fesenko, and R. W. Chantrell, Sci. Rep. **3**, 3262 (2013).

[42] A. Hassdenteufel, J. Schmidt, C. Schubert, B. Hebler, M. Helm, M. Albrecht, and R. Bratschitsch, Phys. Rev. B **91**, 104431 (2015).

[43] R. Medapalli, I. Razdolski, M. Savoini, A. R. Khorsand, A. Kirilyuk, A. V. Kimel, T. Rasing, A. M. Kalashnikova, A. Tsukamoto, and A. Itoh, Phys. Rev. B **86**, 054442 (2012).

[44] R. Medapalli, I. Razdolski, M. Savoini, A. R. Khorsand, A. Kalashnikova, A. Tsukamoto, A. Itoh, A. Kirilyuk, A. Kimel, and T. Rasing, Eur. Phys. J. B **86**, 183 (2013).

[45] L. Le Guyader, S. El Moussaoui, M. Buzzi, M. Savoini, A. Tsukamoto, A. Itoh, A. Kirilyuk, T. Rasing, F. Nolting, and A. V. Kimel, Phys. Rev. B **93**, 134402 (2016).